Supporting Information

Aitken et al. 10.1073/pnas.1519790113

Stress Analysis of Three-Point Bending Experiments

Stresses and strains were calculated along the bottom edge of the beam directly under the point of applied load, which corresponds to the point of maximum tensile stress:

$$\sigma = -\frac{My}{I} \quad [S1]$$

$$\varepsilon = -\frac{y}{\rho}, \quad [S2]$$

where M is the bending moment, y is the perpendicular distance away from the neutral axis of the beam, I is the cross-sectional moment of inertia, and ρ is the radius of curvature (31). At the point of maximum tensile stress, the moment $M = PL/2$ and $= -h/2$, P is the applied load, L is half the span of the gauge section, and h is the height of the beam. The contribution from the cribrum and basal plate to the moment of inertia are $I_{cribrum} = (1/12)h_c^3 w_c$ and $I_{basal} = (1/12)h_b^3 w_b$, respectively, where w is the thickness of the layer and subscripts c and b refer to the cribrum and basal plate. As shown in Fig. S4*D*, the gauge section, $2L$, and the beam height, h, are dimensions that lie within the shell plane and the width w, is perpendicular to the shell plane. Estimation of the contribution to the moment of inertia from the areola lattice can be difficult due to the directionality of the hexagonal cell array. Under this loading configuration, an individual areolae wall has a thickness, $h_{aerola} = 300$ nm and a width, $w_{aerola} = 2.5$ μm, so that $h_{aerola}/h_{cribcrum} \sim 0.1$ and $w_{aerola}/w_{cribcrum} \sim 10$. The predicted contributions to the area moment of inertia from the areolae walls with these dimensions are at least 2 orders of magnitude less than the individual contribution from the cribrum and from the basal plate, which makes it reasonable to exclude the contribution of areolae from the analysis. We observed a small, <3° biaxial curvature in the as-fabricated frustule beam, possibly due to relaxation of residual stresses after its extraction from the frustule. To account for this curvature, the height of the beam was calculated as the average of the two layers measured after sample extraction, $(h_c + h_b)/2$. This results in the following expression for the uniaxial tensile bending stress in the bottom edge of the beam:

$$\sigma_{beam} = \frac{3PL(h_c + h_b)}{2\left(h_c^3 w_c + h_b^3 w_b\right)}. \quad [S3]$$

The beams tested in this work were not fixed to the substrate to avoid generating boundary constraints, so any initial misorientation of the beam or misorientation of the indenter tip with respect to the beam resulted in "settling" events during testing manifested by marginal tilting and translation of the beam before attaining full contact. As a result, the measured indenter displacement could not be used to calculate strain in the sample. Using the acquired video frames, we analyzed 450 still images taken between incipient sample loading up to failure, to track the position of seven points along the bottom edge of the bending sample. A schematic in Fig. 3*A* shows these seven points whose positions were fit to a circle with radius ρ and used to determine the tensile strain as

$$\varepsilon_{beam} = \frac{(h_c + h_b)}{4\rho}. \quad [S4]$$

SEM Imaging Contrast Within Basal Plate

Fig. S1 shows a top-down view of a representative frustule beam. A sharp contrast difference is observed within the basal plate. Fig. S1, *Inset* shows a zoomed-in view of a section of the basal plate to highlight this contrast. This contrast difference was also observed in TEM analysis of the frustule (Fig. 2*A*), suggesting that these regions indicate layers of differing material or microstructure.

FEM Simulations

A computer-aided design model of one of the bending samples was meshed using 729,000 tetragonal elements in Abaqus simulation package 6.14 (Simulia). To emulate three-point bending, the beam was modeled in contact with steel supports on both ends and displacement was applied via a diamond roller from the top. The beam was assumed to have an elastic modulus of 35 GPa, closely matching the experimental value obtained here. The steel supports and diamond roller were assumed to have elastic moduli of 200 GPa and 1,000 GPa, respectively. Nodes on the bottom face of the steel supports were specified to have no displacement and hard, impenetrable contact via penalty enforcement was assumed between the beam and steel supports and between the beam and diamond roller. A friction coefficient of 0.1 was applied between the steel supports and the beam to prevent lateral sliding during bending. Displacement of the diamond roller was chosen such that the resulting maximum tensile beam strain was similar to experimental values calculated from the captured video. For comparison, bending simulations were also performed on a solid beam of similar dimensions and elastic modulus.

Fig. S3 shows the distribution of stress through a three-point bending sample recreated for FEM analysis. The stresses within the areolae region are up to an order of magnitude lower than the stresses supported in either the cribrum or basal layers.

Bending Beam, Nanoindentation, and TEM Sample Fabrication

Fig. S4 shows a graphical description of the procedure to fabricate samples for three-point bending experiments, nanoindentation, and TEM analysis from the diatom shell.

Samples for bending experiments, TEM analysis, and ex situ nanoindentation were fabricated using the focused ion beam (FIB) lift-out technique in a dual-beam SEM (FEI Versa 3D) (32). Once an intact frustule was identified, a cantilever beam with plane dimensions of 3.5 × 24 μm was milled out of the center of the frustule at 16 kV and 0.25 nA. The depth of the beam was set by the thickness of the frustule shell and was ∼3.5 μm. A site-specific, platinum deposition needle and tungsten micromanipulator (FEI EZLift) were used to extract the sample. The micromanipulator was welded to the free end of the cantilever beam using Pt deposition and the opposite end of the cantilever was milled away from the parent frustule. Fig. S4 *A*–*C* show SEM images of this lift-out procedure. The beam was then transferred onto a stainless steel substrate and placed over prefabricated 20- × 20- × 40-μm wells. The same micromanipulator was then used to position the beam such that its gauge section was parallel to the short edge of the well and spanned it entirely, ensuring that the shell plane normal was perpendicular to the loading direction, as shown in Fig. S4*D*. This type of parallel loading allows us to deform all frustule layers simultaneously and removes the complications caused by the compliance differences between layers and the possibility of localized deformation that emerges when the frustule layers are loaded in series (10, 11). This orientation also

limits the influence of the areolae walls and simplifies the calculation of stresses within the beam.

Fabrication of a basal plate for nanoindentation was prepared using the described lift-out technique to extract a 25- × 25-μm plate from the basal diatom plate. The removed plate was then transferred to a copper TEM grid for thinning. The plane of the frustule shell was oriented parallel to the ion beam, and the cribellum, cribrum, and areolae walls were removed using milling conditions of 16 kV and 50 pA, leaving only the basal plate (Fig. S4*E*). Using the tungsten micromanipulator, the basal plate was transferred from the TEM grid to a stainless steel substrate and secured by depositing Pt along the edges of the plate. Decomposition and fracture of the diatom shell during cleaning resulted in several girdle bands suitably oriented for nanoindentation on the substrate, which was performed with no modification to the structure. Fig. 3 *C* and *D* show SEM images of the basal plate and the girdle band used in this study.

Samples for TEM analysis were fabricated using the described lift-out procedure, with the extracted lamella transferred and attached to the Cu TEM grid using the Pt deposition needle in the FIB. The attached TEM samples were then thinned using FIB to a thickness of less than 100 nm using a voltage of 16 kV and progressively decreasing currents from 50 to 11 to 4 pA to ensure electron transparency. A thinned TEM lamella is shown in Fig. S4*F*.

Analysis of Relative Density

We define the relative density of the diatom frustule as the ratio of material volume in the frustule, $V_{frustule}$, to volume in a solid shell of equal dimension, V_{solid}:

$$\rho_{relative} = \frac{V_{frustule}}{V_{solid}} = \frac{V_{cribrum} + V_{areolae} + V_{basal} + V_{rim}}{V_{solid}}, \qquad \textbf{[S5]}$$

where $V_{cribrum}$, $V_{areolae}$, and V_{basal} are the volume of the cribrum, areolae, and basal layers, respectively, and V_{rim} is the volume of the raised foramen rim. Owing to symmetry of the frustule, we start by considering a single hexagonal unit of the frustule as shown in Fig. S2 and develop a general model for the relative density. Fig. S2 *B*–*D* show schematics of the projected area in each layer of the frustule. By defining the relative projected area as the ratio of projected area for a given layer i, A_i, and the solid area, A_{solid}, Eq. **S5** can be rewritten as

$$\rho_{relative} = \frac{A_{cribrum}}{A_{solid}}\frac{w_{cribrum}}{w_{total}} + \frac{A_{areolae}}{A_{solid}}\frac{w_{areolae}}{w_{total}} + \frac{A_{basal}}{A_{solid}}\frac{w_{basal}}{w_{total}} + \frac{A_{rim}}{A_{solid}}\frac{w_{rim}}{w_{total}}, \qquad \textbf{[S6]}$$

where $w_{cribrum}$, $w_{areolae}$, and w_{basal} are the depth of the cribrum, areolae, and basal layers, respectively, and w_{rim} is the thickness of the raised foramen rim. $w_{total} = w_{cribrum} + w_{areolae} + w_{basal} + (1/2)w_{rim}$ is the total depth of the beam.

From the observed hexagonal arrangement of pores in the cribrum, we assume seven cribrum pores per hexagonal unit. The projected area of the cribrum is then given:

$$A_{cribrum} = A_{solid} - \frac{7\pi}{4}d_c^2, \qquad \textbf{[S7]}$$

where d_c is the diameter of a cribrum pore. The total area of the walls that make up the areolae is

$$A_{areolae} = A_{solid} - \frac{3\sqrt{3}}{2}\left(a - \frac{t}{\sqrt{3}}\right)^2, \qquad \textbf{[S8]}$$

where a and t are the length and thickness of the areolae wall, respectively. The area within the basal layer and area of the raised rim are

$$A_{basal} = A_{solid} - \frac{\pi}{4}d_{b,inner}^2 \qquad \textbf{[S9]}$$

$$A_{rim} = \frac{\pi}{4}\left[d_{b,outer}^2 - d_{b,inner}^2\right], \qquad \textbf{[S10]}$$

where $d_{b,inner}$ and $d_{b,outer}$ are the inner and diameter of the foramen rim. Noting that the solid area is simply the area of the hexagonal cell, $A_{solid} = (3\sqrt{3})/2a^2$, Eq. **S6** then gives the final expression for the relative density of the frustule:

$$\rho_{relative} = 1 - \frac{7\pi}{6\sqrt{3}}\left(\frac{d_c}{a}\right)^2\frac{w_{cribrum}}{w_{total}} - \left(1 - \frac{1}{\sqrt{3}}\frac{t}{a}\right)^2\frac{w_{areolae}}{w_{total}} - \frac{\pi}{6\sqrt{3}}\left(\frac{d_{b,\,inner}}{a}\right)^2\frac{w_{basal}}{w_{total}} + \frac{\pi}{6\sqrt{3}}\left[\left(\frac{d_{b,\,outer}}{a}\right)^2 - \left(\frac{d_{b,\,inner}}{a}\right)^2\right]\frac{w_{rim}}{w_{total}}. \qquad \textbf{[S11]}$$

Average measured values for d_c, $d_{b,\,inner}$, and $d_{b,\,outer}$ as well as measured values for $w_{cribrum}$, $w_{areolae}$, w_{basal}, w_{rim}, and w_{total} of each frustule beam are given in Table S1. Average values of t and a taken from 50 measurements of the indentation sample are 0.17 μm and 1.19 μm, respectively. For these values, the average relative density of each frustule beam is calculated and given in Table S1. The average relative density as determined by Eq. **S11** is 36.4%.

By taking advantage of the periodicity of the frustule we have been able to develop a general model, but the simplifying assumptions used could lead to a misrepresentation of the relative density of a beam sample. From SEM imaging it is seen that the pores in the cribrum layer are typically elliptic and vary in number per hexagonal cell and that foramen are not necessarily regularly spaced. Similarly, hexagonal areolae cells are irregular and the number of cell walls can vary from 5 to 6. To test the veracity of this general model, we used direct measurement of SEM images of each frustule beam to calculate $V_{cribrum}$, $V_{areolae}$, V_{basal}, and V_{rim}.

Ellipses were manually fit to each cribrum pore in the beam and the area of each ellipse was summed to provide the pore area, A_{pore}. The inverse area is determined by subtracting the pore area from the rectangular area, A_{beam}. Multiplying by the depth gives the cribrum volume $V_{cribrum}$:

$$V_{cribrum} = w_{cribrum}\left(A_{beam} - A_{pore}\right). \qquad \textbf{[S12]}$$

A similar procedure was used to determine the volume of the basal layer, V_{basal}, by fitting circles to the inner diameter of each foramen:

$$V_{basal} = w_{basal}\left(A_{beam} - A_{foramina}\right). \qquad \textbf{[S13]}$$

The difference in area between circles fit to the outer and inner diameter of each foramen provides the total projected area of the foramen rims, A_{rim}. Multiplying by the average thickness of the foramen rims gives the total rim volume, V_{rim}:

$$V_{rim} = w_{rim}\left(A_{beam} - A_{rim}\right). \qquad \textbf{[S14]}$$

Determination of $V_{areolae}$ is difficult because the areolae walls are obscured by the cribrum and basal layers. To provide an estimation of the location of areolae walls, we generated a Voronoi diagram using the centers of the foramen as the seeds of each cell and bounded by the dimensions of the beam. This method generates a remarkably good match when applied to the visible areolae walls in the indentation plate shown in Fig. 2*E*. $V_{areolae}$ could then be determined from the total length of the cell walls,

$l_{areolae}$ multiplied by the average areolae wall thickness, t and depth of the areolae layer:

$$V_{areolae} = w_{areolae} * l_{areolae} * t. \quad \textbf{[S15]}$$

The solid volume was determined using the average heights and depths of each beam:

$$V_{solid} = \frac{h_{cribrum} + h_{basal}}{2} * \frac{L_{cribrum} + L_{basal}}{2} * w_{total}, \quad \textbf{[S16]}$$

where $L_{cribrum}$ and L_{basal} are the lengths of the cribrum and basal layers, respectively. These volumes were then directly substituted into Eq. **S5** to provide the measured relative density. The volumes $V_{cribrum}$, $V_{areolae}$, V_{basal}, V_{rim}, and V_{solid} and resulting relative densities are shown in Table S2. The average relative density as calculated from direct image measurements was 30.1%, showing decent similarity with the generalized model.

For analysis and discussion in this paper we use the relative density calculated from image measurements as it provides a direct value for each unique beam sample.

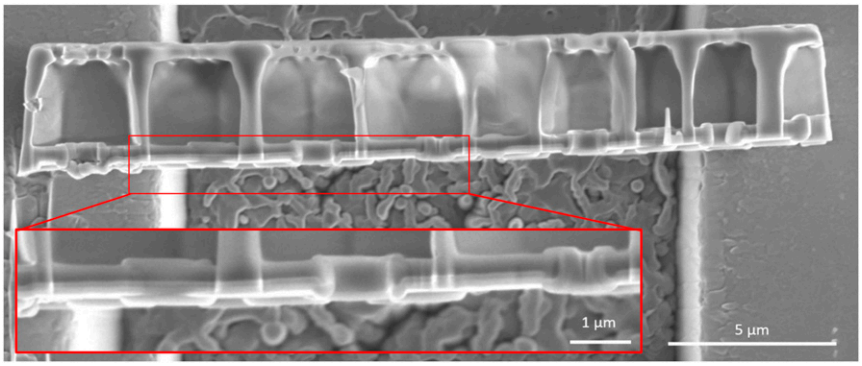

Fig. S1. SEM image giving a top-down view of a representative beam sample. (*Inset*) The sharp contrast difference within the basal plate.

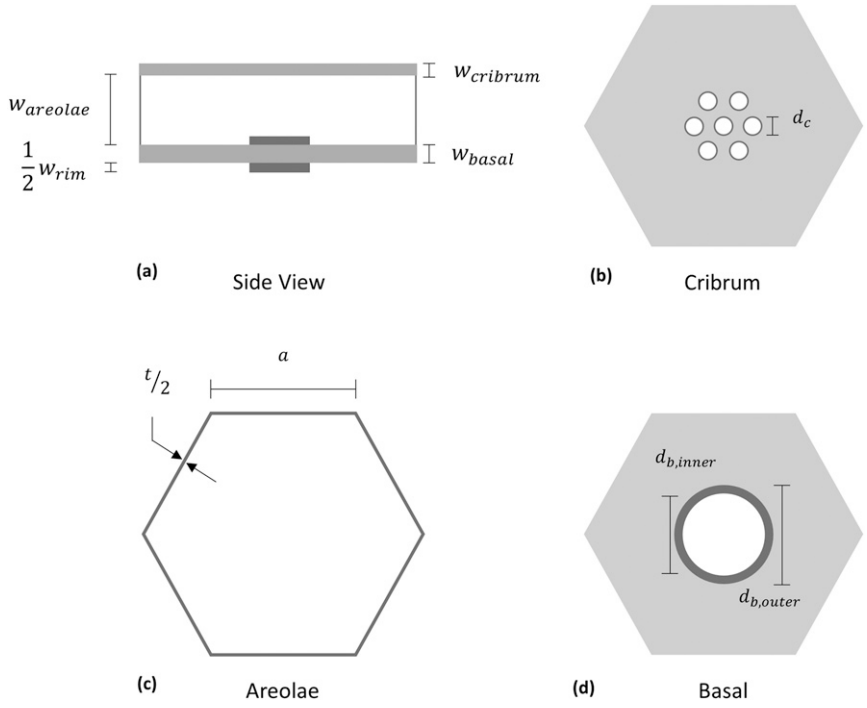

Fig. S2. Schematic showing the hexagonal unit of frustule. (*A*) A cross-section of the frustule shell. (*B–D*) Top-down views of each layer of the frustule shell.

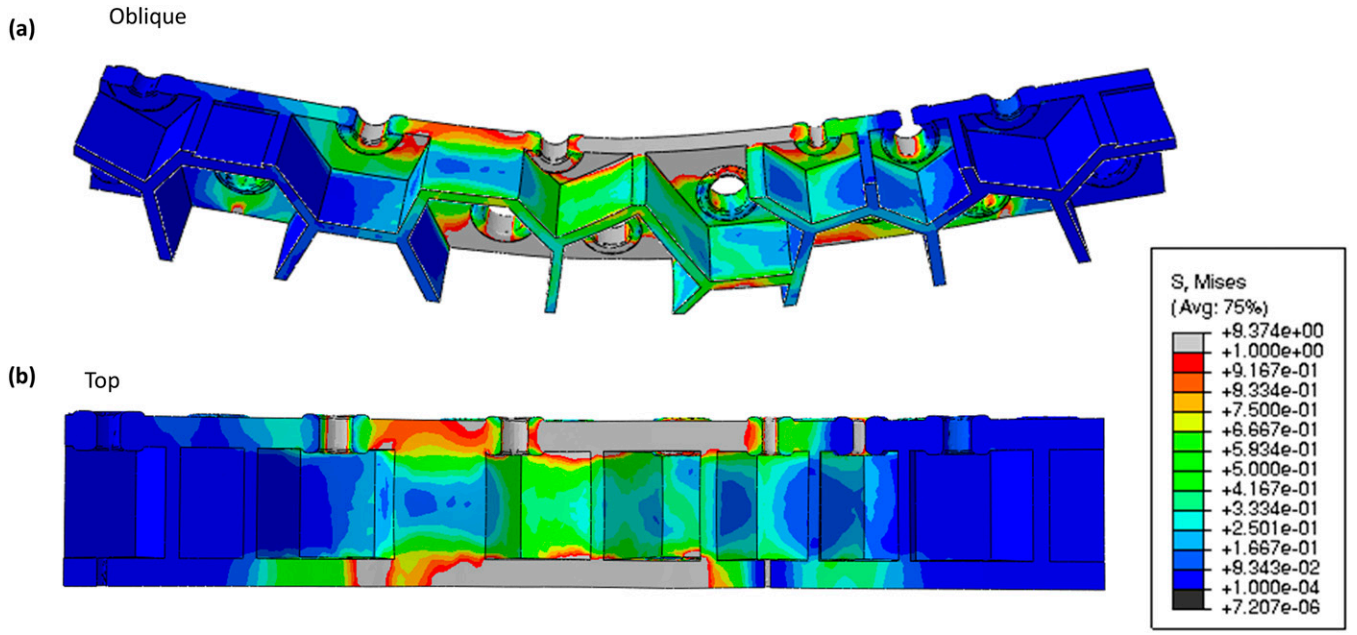

Fig. S3. Displays the von Mises stress distribution throughout the bending beam in an (*A*) oblique view to highlight the stress distribution in the areolae walls and (*B*) top-down view.

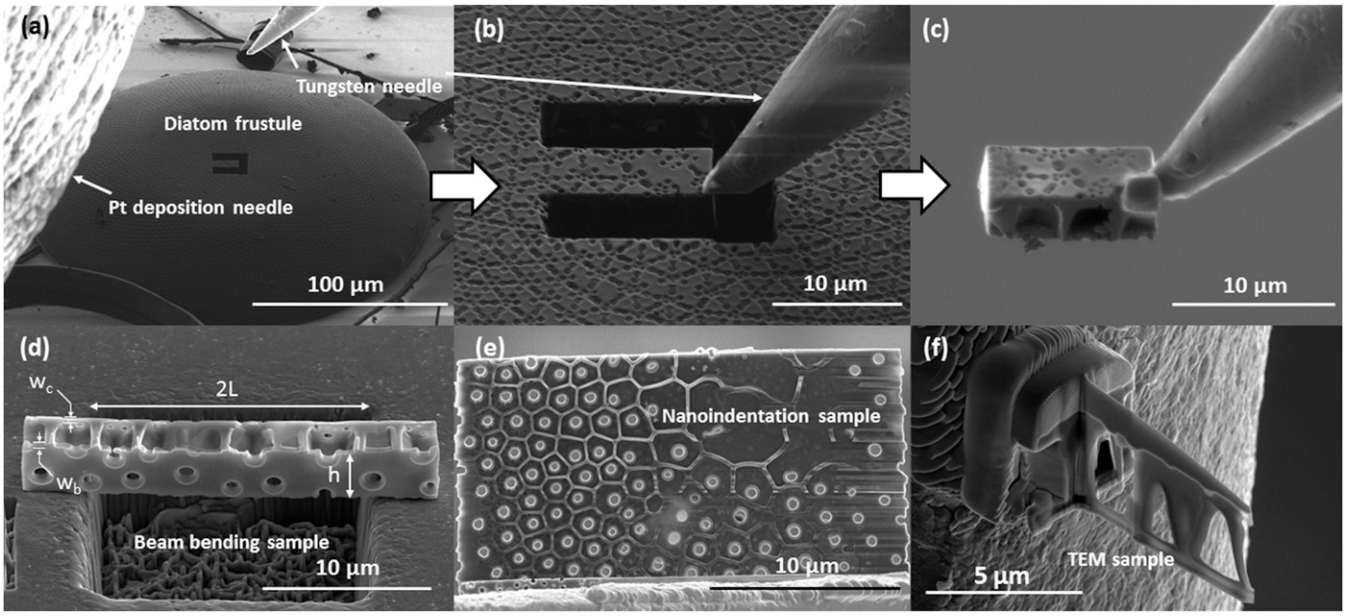

Fig. S4. (*A*–*C*) SEM snapshots demonstrating the focused ion beam lift-out method. The FIB is used to mill out a rectangular sample and a Pt deposition needle is used to attach to the tungsten micromanipulator for lift-out. This technique can be used to prepare (*D*) bending samples, (*E*) nanoindentation samples, and (*F*) TEM lamella from the frustule shell. Dimensions of the beam sample are shown in *D*. The gauge length of the beam is *2L* and the height of beam is *h*. Thickness of the cribrum layer, w_c, and basal layer, w_b, are also shown.

Table S1. Pore dimensions and layer widths used in the general model for relative density

Sample	d_c, μm	$d_{b,\ inner}$, μm	$d_{b,\ outer}$, μm	$w_{cribrum}$, μm	$w_{areolae}$, μm	w_{basal}, μm	w_{rim}, μm	$\rho_{relative}$
1	0.34	0.80	1.47	0.42	2.66	0.62	0.29	0.401
2	0.34	0.82	1.37	0.26	2.97	0.41	0.19	0.314
3	0.35	0.89	1.49	0.36	2.67	0.48	0.28	0.369
4	0.27	0.90	1.43	0.31	1.94	0.32	0.20	0.373
5	0.30	0.70	1.33	0.38	2.49	0.35	0.21	0.360

Table S2. Layer and solid volumes for each beam sample and associated relative density

Sample	$V_{cribrum}$, μm^3	$V_{areolae}$, μm^3	V_{basal}, μm^3	V_{rim}, μm^3	V_{solid}, μm^3	$\rho_{relative}$
1	25.05	20.38	44.80	4.20	280.65	0.336
2	17.98	28.46	35.84	1.38	322.33	0.260
3	38.40	39.75	57.39	5.01	455.15	0.309
4	20.52	16.30	21.80	1.80	196.42	0.308
5	27.84	22.17	28.83	2.51	277.52	0.293